arXiv:1612.05042v1 [astro-ph.SR] 15 Dec 2016

Accuracy of the component mass estimation methods in LMXB.

Antokhina [1*]E. A., Petrov[1] V. S., Cherepashchuk[1] A. M.

[1]Sternberg Astronomical Institute, Moscow M.V. Lomonosov State University

December 16, 2016

Abstract

There is a mismatch between modelled and observed distributions of optical stars masses in BH LMXB. Companion masses in BH LMXB are found in the mass range 0.1 - 1.6 $M_\odot$ with the peak at 0.6 $M_\odot$. The standard evolutionary scenarios require the donor mass distribution peaks to be at least $\sim 1\ M_\odot$ to eject a massive envelope of the black hole progenitor. Imperfect of the methods of optical stars masses determination may cause this difference.

Two common used approximations of real Roche lobe filling star as distortion sources have been tested. On the one hand, there is the a approximation of real Roche lobe filling optical stars as sphere. We tested rotational broadening of absorption lines based on an exact calculation of CaI λ6439.075 Å absorption profiles in the spectra of Roche lobe filling optical stars. There is overestimation of projected equatorial rotational velocity $V_{rot} \sin i$ and, accordingly, underestimation of mass ratio $q = M_x/M_v$ in the spherical star model. On the other hand, the approximation of a real Roche lobe filling star as disk with uniform local profile and linear limb darkening law is more rough. In this case overestimation of projected equatorial rotational velocity $V_{rot} \sin i$ is $\sim 20\%$. Such overestimation of $V_{rot} \sin i$ can result in significant underestimation of mass ratio $q = M_x/M_v$ at hight value of

*elant@sai.msu.ru

$q = M_x/M_v$. Refined value of q does not affect the mass of a black hole, but the mass of an optical star has shrunk 1.5 times. Hence, the masses of optical stars in BH LMXB must be corrected downward, despite the contradictions to the standard evolutionary scenarios.

1 Introduction

There are 26 currently known X-ray binary systems with black holes : 17 with low mass optical companions (LMXB) with $M_v = 0.3 \div 2 M_\odot$ and 9 with high mass optical companions (HMXB) with $M_v = 5 M_\odot - 70 M_\odot$ (Cherepashchuk, 2013). Evolution scenarios for this two groups are completely different. Evolution of BH LMXB leads to the formation of common envelope. After common envelope phase the primary core rapidly evolves towards core collapse and the BH formation. The hight mass x-ray binary system evolved as a detached system. The difference in distribution of the masses of black holes in LMXB and HMXB is shown in Fig. 1. The typical black hole masses in LMXB are around $M_{BH} \simeq 8 M_\odot$. The black hole mass in HMXB is distributed in broad range of masses without any peak.

The standard evolutionary scenarios require the donor mass distribution peaks to be, at least, $\sim 1\ M_\odot$ to eject a massive envelope of the black hole progenitor (Podsiadlowski et al., 2010). The low mass companion with mass below 1 $M_\odot$ has difficulties in ejecting the tightly bound envelope of the massive primary during the spiral-in process. But observational masses in BH LMXB are found in the mass range 0.1 - 1.6 $M_\odot$ with peak at 0.6 $M_\odot$. Wang et al. (2016) use both stellar evolution and binary population synthesis to study the evolutionary history of BH LMXBs. It has been shown that it is possible to form BH LMXBs with optical components masses below $\sim 1\ M_\odot$ and the standard CE scenario if most BHs are born through failed supernovae. But α-elements (O, Si, Mg, etc.), which cannot be produced by nuclear burning in low mass stars were detected in the atmosphere of two LMXB optical components (GRO J1655-40 and SAX J1819.3-2525). Therefore, the predictions are still in tension with available observations.

The mass of black hole in LMXB is given by:

$$M_x = \frac{f_v(M)\,(1+q^{-1})^2}{\sin^3 i}, \qquad (1)$$

where $q = M_x/M_v$, M_x - the mass of the X-ray component, i - the orbital inclination, $f_v(M)$ - the mass function of the optical component. The mass function is derived from:

$$f_v(M) = 1.038 \cdot 10^{-7} K_c^3 P_{orb}(1-e^2)^{3/2}. \quad (2)$$

where K_c - the semi-amplitude of the radial velocity curve of the center of mass of the companion star, P_{orb} - the orbital period, e - the eccentricity. In case of stellar mass black holes ($q = M_x/M_v \gg 1$) mass M_x depends weakly on q (see 1), so we can consider the black hole mass in BH LMXB as a function of the K_c and i. However for the mass of the optical star $M_v = M_x/q$ value of q is significant.

The effects of the asphericity of a star in particular BH LMXB on its rotational broadening of absorption lines was considered by Marsh et al. (Marsh et al., 1994) and Shahbaz (Shahbaz, 2003). Marsh et al. (Marsh et al., 1994) employed both the geometry of Roche lobe and orbital smearing of spectral lines to estimate the mass ratio systematic uncertainty in BH LMXB A0620-00. This uncertainty was about 5%. It needs to be noted that their findings were obtained without full model-atmosphere calculations.

Shahbaz (Shahbaz, 2003) found mass ratio q in Nova Sco 1994 (the F star) fitting the observed high quality spectrum with synthetic spectra. Author made direct use of NextGen atmosphere models which take into account the varying temperature and gravity across the secondary star's photosphere, by incorporating the synthetic spectra into the secondary star's Roche geometry. This method of determination of the mass ratio does not depend on assumptions about the rotation profile and limb darkening coefficients. Also the author performed the calculations of mass ratio with star's model as disk with uniform local profile and linear limb darkening law so-called classical rotational broadening model (Collins & Truax, 1995). The calculations for two different values of limb-darkening coefficients showed that the Roche-model gives a mass ratio that lies in between the values obtained using limb-darkening coefficients of zero and 0.52 (continuum).

Antokhina and Cherepashchuk (Antokhina & Cherepashchuk, 1997) also investigated tidal distortion effect on mass ratio determination using rotational broadening of absorption lines. They showed that neglecting the pear-like shape of the star leads to underestimation of the component-mass ratio $q = M_x/M_v$, i.e., to overestimation of the mass of the black hole in the system.

In this paper, the accuracy of two widely used approximations of optical star in LMXB mass ratio estimation (spherical model and classical rotational broadening model) has been compared.

2 The method of mass ratio estimation by rotational broadening of absorption lines

If the orbit is circular and the star's rotation is synchronized with the orbital motion, the following kinematic relation is satisfied (Cherepashchuk, 2013; Wade & Horne, 1988):

$$V_{rot} \sin i = K_c \left(1 + \frac{1}{q}\right) \frac{r_v}{a}. \tag{3}$$

Here, $q = M_x/M_v$ is the ratio of the masses of the relativistic object and the optical star in the binary, K_c the semi-amplitude of the radial velocity curve for the center of mass of optical star, r_v is mean star radius, a is the radius of the circular orbit, V_{rot} is the equatorial rotational velocity, and i is the orbital inclination.

Paczynski (Paczynski, 1971) proposed an approximate analytical expression for calculating the radius of a sphere with a volume equal to one of the critical Roche lobe:

$$\frac{\bar{R}}{a} \simeq 0.462 \ (1+q)^{-1/3}. \tag{4}$$

The $\bar{R}$ value is usually called the "mean radius of the Roche lobe." Formulas (3) and (4) can be used to derive the formula that was first presented by Wade and Horne (Wade & Horne, 1988):

$$\frac{V_{rot} \sin i}{K_c} \simeq 0.462 \ q^{-1/3} \left(1 + \frac{1}{q}\right)^{2/3}. \tag{5}$$

The expression (5) is widely used to determine the component-mass ratios q in binary systems based on the rotational broadening of lines (see, e.g. Marsh et al. (1994); Casares & Charles (1994)). The more exact formula of Eggleton (Eggleton, 1983) can also be used for the mean radius of the Roche lobe, but formula (5) will be used further in the calculations. It is

necessary to mention that in the limit case where $q = M_x/M_v >> 1$ (this case corresponds to BH LMXB) mass ratio q is given by:

$$q \simeq \left(\frac{0.462 K_c}{V_{rot} \sin i} \right)^3 . \quad (6)$$

It follows from the expression (6) that small uncertainties in $V_{rot} \sin i$ lead to large uncertainties in q.

Marsh et al. (Marsh et al., 1994) and Casares & Charles (Casares & Charles, 1994) determined the rotational broadening of line profiles in the spectra of the optical components of X-ray binary systems. They used the observed line profiles for slowly rotating stars with close spectral types (reference stars) as profiles unbroadened by rotation. The spectra of the stars in the X-ray binaries and those of the single slowly rotating stars were obtained with the same spectral resolution. The rotational broadening of the spectra of the reference stars was modelled, assuming that these profiles would be the same in the absence of rotation, identifying the value of $V_{rot} \sin i$ for which the spectra of the single star and the star in the X-ray binary were in best agreement with χ^2 criterion. In this way, the rotational velocity $V_{rot} \sin i$ of the star in the binary system was found. This approach made it possible not to correct the influence of the instrumental function of the spectrograph.

Two methods, i.e the minimum value of χ^2 and equality of Full Width Half Maximum ($FWHM$) for CaI λ6439.075 Å line profiles, have been employed to estimate $V_{rot} \sin i$. In our current study, we computed both the minimum value of χ^2 and equality of Full Width Half Maximum ($FWHM$) for CaI λ6439.075 Å line profiles. We found that difference in determination of $V_{rot} \sin i$ by these two methods do not exceed 2%. Therefore, we use $FWHM$ equality method.

3 The spherical star approximation

We used the computational method proposed by Antokhina et al. (Antokhina et al., 2005) to correctly model theoretically the line profiles emitted by optical stars in close X-ray binary systems. It is necessary to describe this algorithm briefly. The computation of the theoretical line profiles and radial velocity curves is carried out using the synthesis method. The tidally deformed stellar surface in the Roche model is divided into thousands of area elements.

The flux of emergent radiation is calculated for each area, taking into account gravitational darkening, heating of the surface by incident radiation from the companion (the reflection effect), and limb darkening. The local line profile for an area element is calculated by constructing an atmosphere model for the given point of the stellar surface. The spectrum of the external radiation from the compact source is specified using X-ray observations or a model function.

Thus, an atmosphere model is calculated at each point of the stellar surface, for specified values of T_{loc}, g_{loc}, and k_x^{loc}, by solving the radiative transfer equation in the line in the presence of the incident external X-ray flux (Antokhina et al., 2005). The adopted model atmosphere is then used to calculate the intensity of the emergent line and continuum radiation, i.e., the line profile for each area element. At each orbital phase, the line is summed over the visible surface of the star, taking into account the Doppler effect, and the integrated line profile from the stellar disk is constructed.

We calculated the "accurate" theoretical CaI λ6439.075 Å profiles and the radial velocity curves using the code Antokhina et al. (2005) for fixed set of parameters: masses M_x, M_v, Roche lobe filling factor $\mu = 1$, the effective temperature of the optical star T_{eff}, the orbital inclination i, e.t.c. at 20 different orbital phases.

The projected rotational velocity of Roche lobe filling star $V_{rot}^{Roche} \sin i$ is one of the output parameter of our calculation. Note that $V_{rot}^{Roche} \sin i$ in current orbital phase is a projected rotational velocity of spherical star with equal volume. We determined $FWHM$ of "true" theoretical profiles in each orbital phase and average over orbital period (phase $\phi = 0$ corresponds to the eclipse of the X-ray source by the optical star). The shape and $FWHM$ of the profiles depend on orbital phase since the projection of the Roche lobe filling star onto the plane of the sky has various areas (Antokhina & Cherepashchuk, 1997).

We estimated the rotational broadening and mass ratio q by fitting "true" theoretical profiles with the spherical star approximation to obtain accuracy of mass ratio determination. Such mass ratio will be denoted as q_{sph}.

The results of modelling using code Antokhina et al. (2005) are listed in Table 1 - 4. We consider the optical star with mass $M_v = 0.8\ M_\odot$ and the effective temperature $T_{eff} = 5000\ K$. The Roche lobe filling factor of the stars is taken to be $\mu = 1$. The orbital inclination is set to be $i = 90^o$. To illustrate the effect of the inclination angle we have also computed the parameters of LMXB for $i = 45^o$ (see table 4). The effect of X-ray heating

is ignored $k_x = L_x/L_v^{bol} = 0$. The mass ratio is in the range of $q = 1 - 40$, and the period is taken to be $P_{orb} = 1, 2, 4$ d.

In the table 1 $\bar{R}$ is the mean radius of the Roche lobe, $\bar{g}$ is the mean surface gravity, a is the radius of the circular orbit, K_v is is the semi-amplitude of the stellar radial velocity curve in the Roche model, K_c is the semi-amplitude of the radial velocity curve of the stellar barycenter. It is important to emphasize that the mean radius of the Roche lobe $\bar{R}$ was defined by integration over the Roche lobe volume in Table 1 - 4. Parameter V_{rot} is the accurate value rotational velocity of Roche lobe filling star.

It is shown in Table 1 - 4 that varying the mass ratio with fixed period P_{orb} leads to the change of the radius of the the circular orbit a, accordingly, to the change of the semi-amplitude radial velocity curve K_c

The variation of mean radius and rotational velocity is very small. In this way mass ratio q is a function of semi-amplitude of the stellar radial velocity curve K_c. We fixed the radius of the circular orbit a, varied P_{orb} and list the parameters in Table 5

We introduce a Cartesian coordinate system (X, Y,Z) with its origin at the center of mass of the optical star. The X axis is directed along the line passing through the component centers, the Y axis lies in the orbital plane, and the Z axis is perpendicular to the orbital plane (see Antokhina & Cherepashchuk (1994, 1997)). Then r_{point} and r_{back} are the points of intersections of the Roche lobe with OX axis. Distances between center of mass of the optical star and of intersections of the Roche lobe with OY and OZ axes are r_{side} and r_{pole} respectively. We list the geometrical parameters of the optical star for $q = 1 - 40$ in Table 6. The elongation along the centers of mass is r_{point}/r_{pole} is also shown.

The goal of our study is determination of rotational broadening of theoretical CaI λ6439.075 Å profiles using two models of optical star. We consider the spherical star model in the first place. Using code Antokhina et al. (2005), we iterated $V_{rot} \sin i$ for spherical star model at which Roche lobe filling and spherical star's line profiles have the same $FWHM$. If the star is spherical the line profile is independent of the orbital inclination i and orbital phase ϕ. However, such a dependence arises for a star that fills its Roche lobe and has a tidally deformed (pear-like) shape.

We list in table 7 results of our calculation of V_{rot} for the spherical star model. We consider the optical star with mass $M_v = 0.8\ M_\odot$ and the effective temperature $T_{eff} = 5000\ K$. The Roche lobe filling factor of the stars is taken to be $\mu = 1$. The orbital inclination is set to be $i = 90^o,\ 45^o,\ 60^o,\ 70^o$ and

90^o. The effect of X-ray heating is ignored $k_x = L_x/L_v^{bol} = 0$. The mass ratio is in the range of $q = 1 - 40$, and the period is taken to be $P_{orb} = 2$ d. The mass ratio q_{sph} founded by the formula (5) also given in table 7.

The line is maximally broad (the $FWHM$ is maximum) in the absence of X-ray heating ($k_x = 0$) at quadrature (phase $\phi = 0.25$) since the projection of the star onto the plane of the sky has its maximum area. Therefore, the spherical star model has the highest value of $V_{rot} \sin i$ this orbital phase. Hence, the value of q_{sph} is less than q according the equation (5). For the case of $\phi = 0$ (phase $\phi = 0$ corresponds to the eclipse of the X-ray source by the optical star) the projection of the star onto the plane of the sky has its minimum and the value of q_{sph} is higher than q. The phase-averaged values of q_{sph} is less then "true" theoretical $q = M_x/M_v$. The deviation between q_{sph} and q is small (is lower then 5%) in the case of small value of $q = M_x/M_v$. However, the deviation reaches 10% in the case of high value of $q = M_x/M_v$ due to a strongly nonlinearity of the equation (5). The difference between q_{sph} and $q = M_x/M_v$ is

$$\Delta q = q - q_{sph}$$

The Fig 2 shows how the mass ratio q_{sph} estimated from spherical star model starts to deviate from "accurate" theoretical $q = M_x/M_v$.

4 The classical rotational broadening model

A rougher method is commonly used (see e.g. Marsh et al. (1994); Casares & Charles (1994)). Let a line with central wavelength λ_0 have a profile $I_{loc}(\lambda - \lambda_0)$, and not be subject to Doppler broadening, with the line profile being constant over the stellar disk. The profile of a line emitted by a star rotating with velocity $V_{rot} \sin i$ is given by (Shajn & Struve, 1929; Carrol, 1933; Collins & Truax, 1995):

$$I_{Dop}(\lambda - \lambda_0) = \int_{-1}^{+1} I_{loc} \left(\lambda - \lambda_0 - \lambda_0 x \, \frac{V_{rot}}{c} \sin i \right) \cdot A(x) dx. \qquad (7)$$

Here, i is the orbital inclination, c is the speed of light, and $A(x)$ is the rotational broadening function, which indicates how the profile of an infinitely narrow absorption line in the stellar spectrum is transformed by the Doppler effect due to rotation.

We take the limb darkening of the stellar disk to be described by the linear law:

$$I(\vartheta) = I(0)(1 - u + u\cos\vartheta), \tag{8}$$

where u is the linear limb-darkening coefficient, ϑ is the angle between the normal to the stellar surface at a given point and the direction toward the observer, and $I(0)$ is the intensity emitted per unit area at the center of the stellar disk. The function $A(x)$ then has the form (see e.g. Gray (2005)):

$$A(x) = C_1 \cdot \sqrt{(1-x)^2} + C_2 \cdot (1 - x^2). \tag{9}$$

where

$$C_1 = \frac{2(1-u)}{\pi(1-u/3)}. \tag{10}$$

$$C_2 = \frac{u}{2(1-u/3)}. \tag{11}$$

Following the prescription of previous chapter we found $V_{rot}^{disk}\sin i$ and q_{disk} have the same $FWHM$ for classical rotational broadening model at which Roche lobe filling star's line profile and the line profile of a template star, had been convolved with the standard rotation profile, . The accuracy of the method is the difference between derived value q_{disk} and fixed "true" value q. We use theoretical CaI λ6439.075 Å profile for orbital inclination $i = 0^o$, $T_{eff} = 5000\ K$ and Roche lobe filling factor $\mu = 0.5$ as an unbroadened profile in the spectra of non-rotating template star. The linear limb-darkening coefficient $u = 0.66$ was assumed in deriving the rotational broadening, based on the work of Al-Naimiy (Al-Naimiy, 1978). To perform convolution with the standard rotation profile we used PyAstronomy 0.9 software (`rotBroad` function). Table 8 lists the results of V_{rot}^{disk} and q_{disk} calculations. We also added the 'true" values of V_{rot}^{Roche} for comparison with V_{rot}^{disk} in table 8. It can be seen that V_{rot}^{disk} is completely higher than the V_{rot}^{Roche}. The deviation between V_{rot}^{disk} and V_{rot}^{Roche} can reach $\sim 20\%$ at high value of $q = M_x/M_v$. These estimates V_{rot}^{disk} correspond to the q_{disk} that is less than q (see eq. (5)). We have calculated the Δq correction for both

linear (dashed line) and non linear fitting (solid line) as it is shown in Fig. 3. Hence, for a given mass ratio q_{disk} the correction Δq is provided by:

$$\Delta q = (0.41 \pm 0.01) {q_{disk}}^{1.224 \pm 0.008}, \tag{12}$$

or the more rough linear fitting:

$$\Delta q = (0.85 \pm 0.03) q_{disk} - (0.94 \pm 0.28) \tag{13}$$

As a second step we explore the effect of T_{eff} variation in the accuracy of q_{disk}. Our calculation is showed that equations (12 - 13) are accurate to better than 5 % in effective temperature range 4000 - 8000 K, and better than 1.5 % in effective temperature range 5000 - 7000 K. The limb-darkening coefficient varied in accordance with the effective temperature of the star T_{eff} (Al-Naimiy, 1978).

The linear limb-darkening coefficient that we have used in eq. (7) is appropriate to the continuum and may not apply to CaI λ6439.075 Å absorption line (Collins & Truax, 1995). We try choose limb-darkening coefficient to offset V_{rot}^{disk}. We have computed the theoretical CaI λ6439.075 Å profiles in a Roche model using the code Antokhina et al. (2005) for fixed set of parameters $q = M_x/M_v = 10$, $i = 90^o$, $P = 1$ d and obtain $FWHM_{mean} = 3.685$ Å and $V_{rot} = 90.46$ km/s (see table 1). This value is plotted in Fig. 4 in dashed line. From Fig. 4 it can be seen that there are no values of the linear limb-darkening coefficient u in the range from 0 to 1 that allow to offset V_{rot}^{disk} for CaI λ6439.075 Å absorption line if we fixed $FWHM$.

5 Conclusions

We compare the accuracy of the mass ratio q determination using two models of optical star in BH LMXB: the spherical star model and the classical rotational broadening model. We use the theoretical CaI λ6439.075 Å profiles in the Roche model computed with code Antokhina et al. (2005) as "observed" line profiles. As in the case of spherical star the integrated line profile is constructed by solving the radiative transfer equation like in the case the Roche model of optical star.

As a result, we determine the corrections Δq to mass ratio $q = M_x/M_v$. In both cases the mass ratios estimated from star models are lower than "true" theoretical $q = M_x/M_v$. But in the case of spherical star model the deviation

between q_{sph} and q reaches 10% only. Hoverer, in the case of the classical rotational broadening model the deviation between q_{disk} and $q = M_x/M_v$ can reach 1.5 times at high value of $q = M_x/M_v \geq 30$ (see Fig. 5). Note, there are no values of the linear limb-darkening coefficient u in the range from 0 to 1 that allow to offset q_{disk} for CaI λ6439.075 Å absorption line.

References

Al-Naimiy H., 1978, Astrophysics and Space Science, 53, 181

Antokhina E., Cherepashchuk A., 1994, Astronomy Reportsl, 38, 367

Antokhina E., Cherepashchuk A., 1997, Astronomy Letters, 23, 773

Antokhina E., Cherepashchuk A., Shimanskii V., 2005, Astronomy Report, 49, 109

Carrol J., 1933, MNRAS, 93, 680

Casares J., Charles P., 1994, MNRAS, 271, L5

Cherepashchuk A. M., 2013, Close Binary Stars. Fizmatlit, Moscow

Collins G., Truax R., 1995, ApJ, 439, 860

Eggleton P., 1983, ApJ, 268, 368

Gray D. F., 2005, The Observation and Analysis of Stellar Photospheres, 3 edn. Cambridge University Press, Ontario

Marsh T., Robinson E. L., Wood J. H., 1994, MNRAS, 266, 137

Paczynski B., 1971, ARA&A, 9, 183

Podsiadlowski P., Ivanova N., Justham S., Rappaport S., 2010, MNRAS, 406, 840

Shahbaz T., 2003, MNRAS, 339, 1031

Shajn G., Struve O., 1929, MNRAS, 89, 222

Wade R., Horne K., 1988, ApJ, 324, 411

Wang C., Jia K., Li X.-D., 2016, arxiv:1601.02721

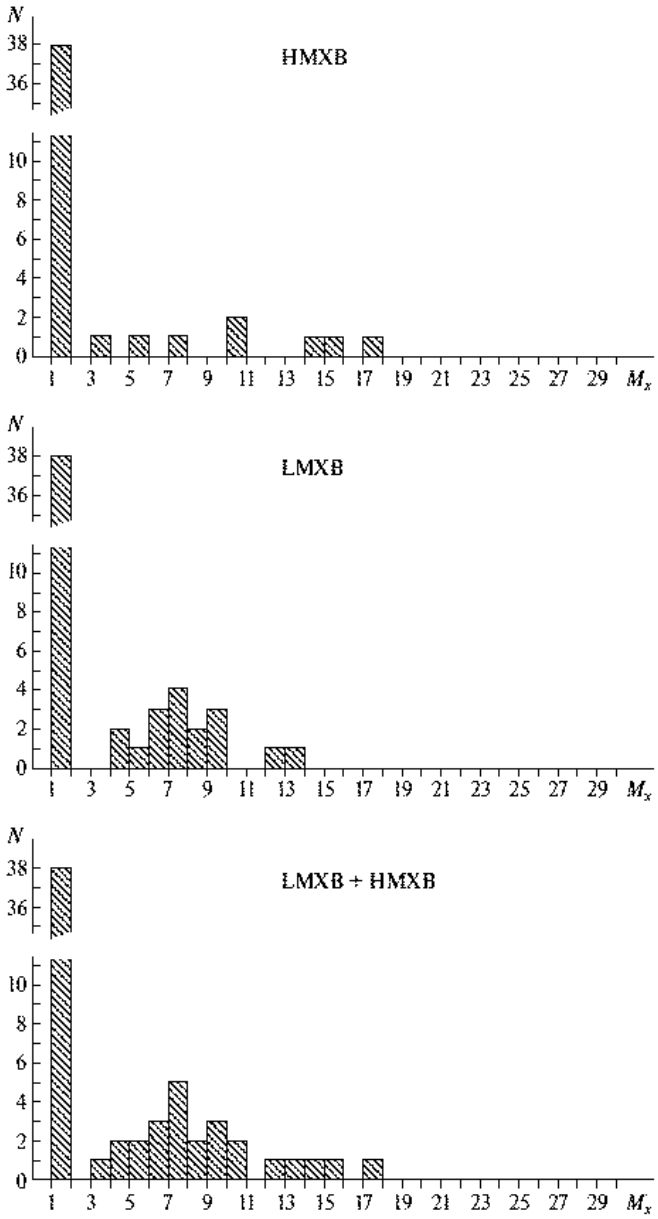


Figure 1: Mass distributions for neutron stars (high peak to the left) and black holes in high-mass and low-mass X-ray binaries.

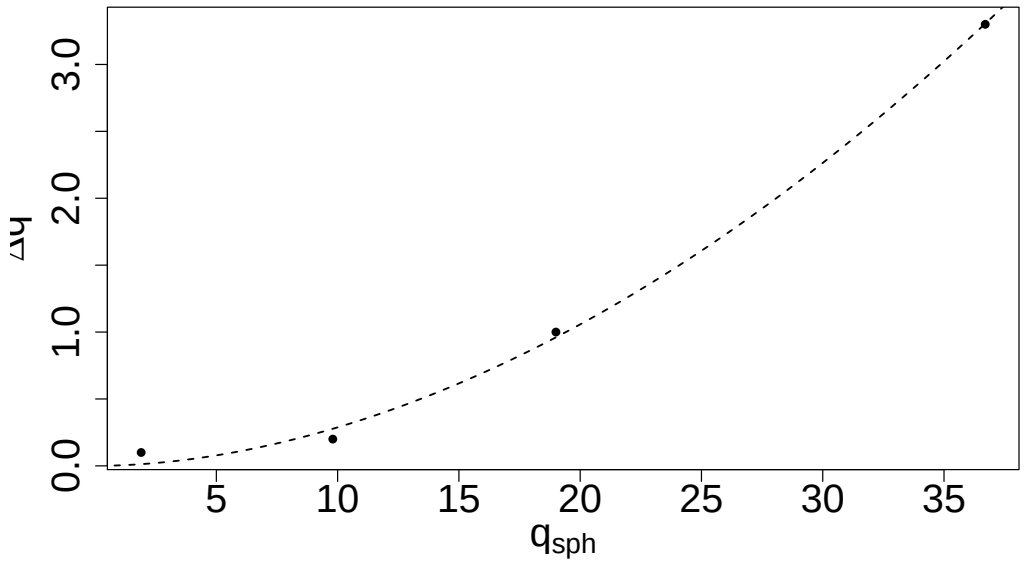


Figure 2: Δq correction as a function of mass ratio q_{sph} in case of the spherical star approximation. Corrected q is expressed by formula $q = q_{sph} + \Delta q$.

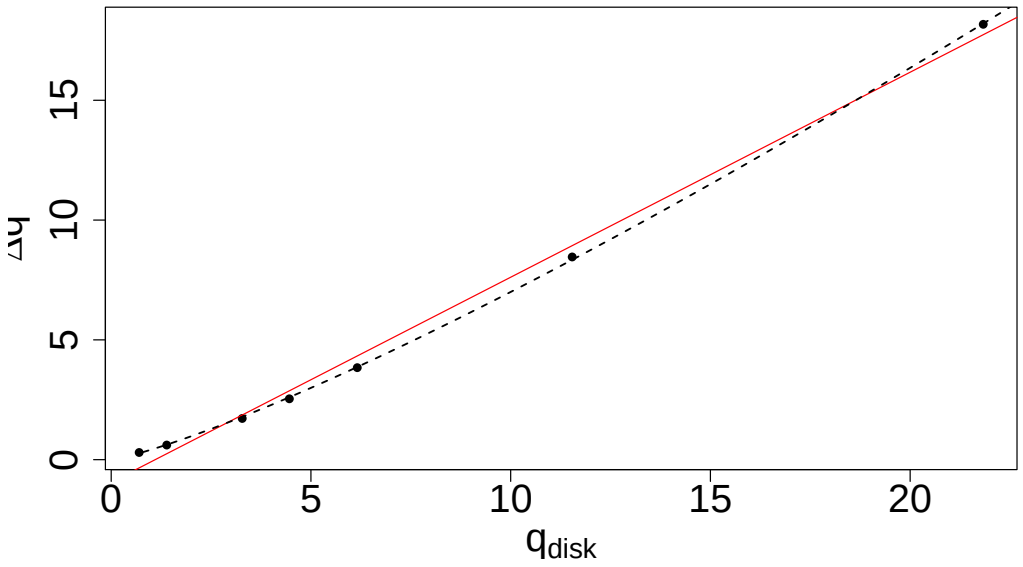


Figure 3: Δq correction as a function of mass ratio q_{disk} in case of the classical rotational broadening model. Solid line represent the linear fitting. A more realistic non-linear fitting represented by a dashed line. Corrected q is expressed by formula $q = q_{disk} + \Delta q$.

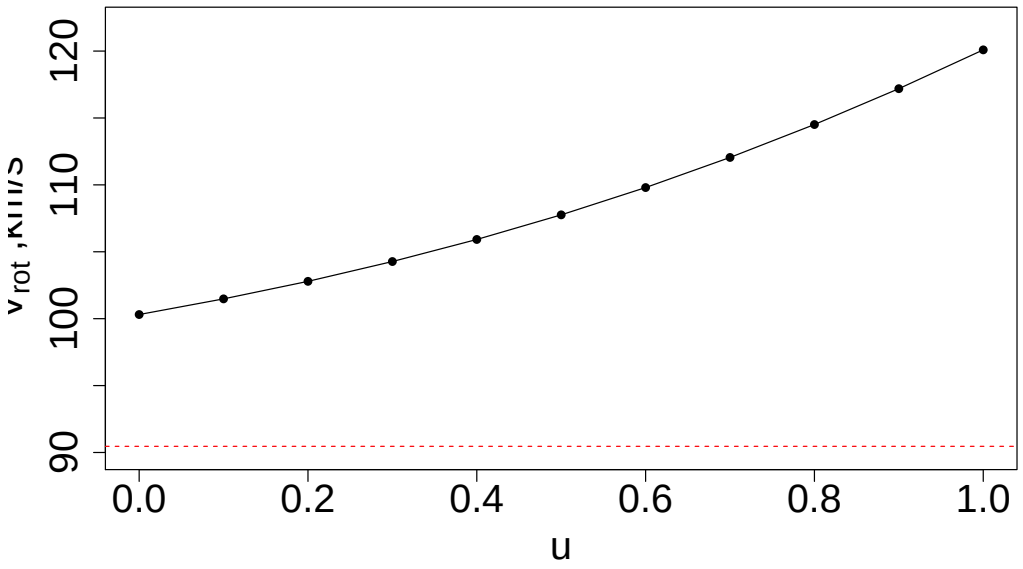


Figure 4: The projected equatorial rotational velocity $V_{rot}^{disk} \sin i$ restored in the framework of classical rotational broadening model with the linear limb-darkening coefficient u. Note that the $FWHM$ of the "observed" line profiles have been fixed ($FWHM = 3.685$ Å). Dashed line represent the $V_{rot} = 90.41$ km/s obtained in a Roche model.

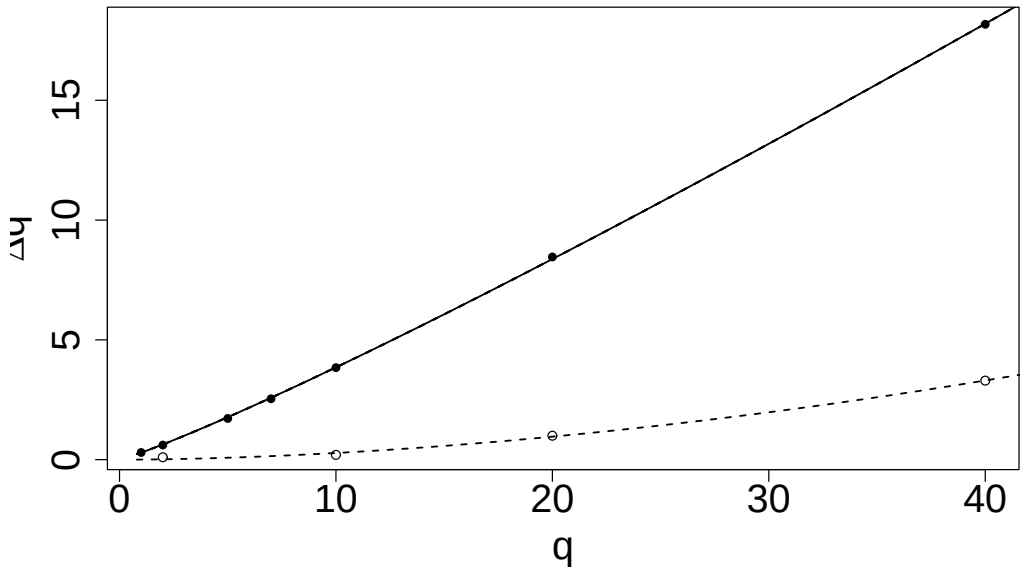


Figure 5: Correction Δq as a function of q (modelled value) for the spherical star model (dashed) and the classical rotational broadening model (solid).

Table 1: Input and derived parameters for $P_{orb} = 1$ d and $i = 90^o$ (the mass ratio varies in the range $q = 1 - 40$)

Parameter	$q = 1$	$q = 2$	$q = 5$	$q = 7$	$q = 10$	$q = 20$	$q = 40$
M_v $(M_\odot)$	0.8	0.8	0.8	0.8	0.8	0.8	0.8
M_x $(M_\odot)$	0.8	1.6	4.0	5.6	8.0	16.0	32.0
P_{orb} (d)	1	1	1	1	1	1	1
a $(R_\odot)$	4.93	5.64	7.11	7.82	8.70	10.79	13.49
$\log \bar{g}$	3.762	3.795	3.808	3.808	3.805	3.796	3.786
$\bar{R}$ $(R_\odot)$	1.87	1.81	1.78	1.78	1.79	1.80	1.82
K_v (km/s)	123.58	189.03	298.45	345.10	398.84	518.85	664.93
K_c (km/s)	124.72	190.36	299.81	346.48	400.29	520.22	666.05
V_{rot} (km/s)	94.77	91.58	90.19	90.23	90.46	91.24	92.18
			CaI λ6439.075 Å line				
$FWHM_{\phi=0.0}$ (Å)	3.780	3.629	3.554	3.549	3.552	3.569	3.594
$FWHM_{\phi=0.25}$ (Å)	3.940	3.829	3.792	3.804	3.823	3.864	3.903
$FWHM_{mean}$ (Å)	3.863	3.729	3.673	3.675	3.685	3.717	3.755

Table 2: Input and derived parameters for Roche model (the mass ratio varies in the range $q = 1 - 40$, $P_{orb} = 2$ d and $i = 90^o$)

Parameter	$q = 1$	$q = 2$	$q = 5$	$q = 7$	$q = 10$	$q = 20$	$q = 40$
M_v $(M_\odot)$	0.8	0.8	0.8	0.8	0.8	0.8	0.8
M_x $(M_\odot)$	0.8	1.6	4.0	5.6	8.0	16.0	32.0
P_{orb} (d)	2	2	2	2	2	2	2
a $(R_\odot)$	7.82	8.96	11.28	12.42	13.81	17.13	21.41
$\log \bar{g}$	3.336	3.393	3.407	3.406	3.404	3.395	3.385
$\bar{R}$ $(R_\odot)$	2.97	2.87	2.83	2.83	2.84	2.86	2.89
K_v (km/s)	98.03	150.04	236.82	273.89	316.63	411.84	527.65
K_c (km/s)	98.99	151.09	237.96	275.00	317.71	412.90	528.65
V_{rot} (km/s)	75.22	72.69	71.59	71.61	71.80	72.42	73.16
			CaI λ6439.075 Å line				
$FWHM_{\phi=0.0}$ (Å)	3.003	2.892	2.819	2.815	2.817	2.833	2.857
$FWHM_{\phi=0.25}$ (Å)	3.166	3.079	3.049	3.057	3.072	3.113	3.154
$FWHM_{mean}$ (Å)	3.078	2.972	2.927	2.928	2.936	2.996	2.996

Table 3: Input and derived parameters for Roche model (the mass ratio varies in the range $q = 1 - 40$, $P_{orb} = 4$ d and $i = 90^o$)

Parameter	$q = 1$	$q = 2$	$q = 5$	$q = 7$	$q = 10$	$q = 20$	$q = 40$
M_v $(M_\odot)$	0.8	0.8	0.8	0.8	0.8	0.8	0.8
M_x $(M_\odot)$	0.8	1.6	4.0	5.6	8.0	16.0	32.0
P_{orb} (d)	4	4	4	4	4	4	4
a $(R_\odot)$	12.42	14.22	17.91	19.71	21.92	27.19	33.99
$\log \bar{g}$	2.959	2.992	3.01	3.005	3.002	2.994	2.983
$\bar{R}$ $(R_\odot)$	4.72	4.56	4.49	4.49	4.50	4.54	4.59
K_v (km/s)	77.77	119.03	187.98	217.38	251.27	326.86	418.84
K_c (km/s)	78.57	119.92	188.87	218.27	252.17	327.72	419.59
V_{rot} (km/s)	59.70	57.69	56.82	56.84	56.99	57.48	58.07
			CaI λ6439.075 Å line				
$FWHM_{\phi=0.0}$ (Å)	2.380	2.290	2.233	2.230	2.231	2.244	2.264
$FWHM_{\phi=0.25}$ (Å)	2.521	2.443	2.423	2.429	2.442	2.476	2.509
$FWHM_{mean}$ (Å)	2.443	2.359	2.323	2.324	2.331	2.353	2.380

Table 4: Input and derived parameters for Roche model (the mass ratio varies in the range $q = 1 - 40$, $P_{orb} = 4$ d and $i = 45^o$)

Parameter	$q = 1$	$q = 2$	$q = 5$	$q = 7$	$q = 10$	$q = 20$	$q = 40$
M_v $(M_\odot)$	0.8	0.8	0.8	0.8	0.8	0.8	0.8
M_x $(M_\odot)$	0.8	1.6	4.0	5.6	8.0	16.0	32.0
P_{orb} (d)	4	4	4	4	4	4	4
a $(R_\odot)$	12.42	14.22	17.91	19.71	21.92	27.19	33.99
$\log \bar{g}$	2.959	2.992	3.01	3.005	3.002	2.994	2.983
$\bar{R}$ $(R_\odot)$	4.72	4.56	4.49	4.49	4.50	4.54	4.59
K_v (km/s)	54.86	84.11	132.85	153.66	177.66	231.02	296.01
K_c (km/s)	55.56	84.80	133.55	154.34	178.31	231.73	296.69
$V_{rot}(km/s)$	59.70	57.69	56.82	56.84	56.99	57.48	58.07
			CaI λ6439.075 Å line				
$FWHM_{\phi=0.0}$ (Å)	1.646	1.580	1.543	1.542	1.543	1.553	1.566
$FWHM_{\phi=0.25}$ (Å)	1.770	1.722	1.708	1.715	1.723	1.744	1.766
$FWHM_{mean}$ (Å)	1.718	1.658	1.635	1.636	1.642	1.658	1.676

Table 5: Input and derived parameters for $P_{orb} = 4$ d and $i = 45^o$ ($q = 1-40$, $a = 12.42\ R_\odot$ and $i = 90^o$)

Parameter	$q=1$	$q=2$	$q=5$	$q=7$	$q=10$	$q=20$	$q=40$
$M_v\ (M_\odot)$	0.8	0.8	0.8	0.8	0.8	0.8	0.8
$M_x\ (M_\odot)$	0.8	1.6	4.0	5.6	8.0	16.0	32.0
$P_{orb}\ (d)$	4.0	3.266	2.310	2.0	1.705	1.234	0.883
$a\ (R_\odot)$	12.42	12.42	12.42	12.42	12.42	12.42	12.42
$\log \bar{g}$	2.959	3.324	3.324	3.406	3.496	3.675	3.858
$\bar{R}\ (R_\odot)$	4.72	3.98	3.114	2.83	2.55	2.07	1.677
$K_v\ (km/s)$	77.77	127.4	225.81	273.89	333.96	483.72	692.92
$K_c\ (km/s)$	78.57	128.31	226.8	275.0	335.07	485.01	694.15
$V_{rot}(km/s)$	59.70	61.72	68.23	71.61	75.72	85.06	96.06
			CaI λ6439.075 Å line				
$FWHM_{\phi=0.0}$ (Å)	2.380	2.444	2.694	2.815	2.974	3.334	3.750
$FWHM_{\phi=0.25}$ (Å)	2.521	2.611	2.911	3.057	3.234	3.618	4.075
$FWHM_{mean}$ (Å)	2.443	2.524	2.792	2.928	3.095	3.472	3.912

Table 6: The relative radii of a star filling its Roche lobe for $q = 1 - 40$

parameter	$q=1$	$q=2$	$q=5$	$q=7$	$q=10$	$q=20$	$q=40$
r_{point}/a	0.5000	0.4291	0.3414	0.3119	0.2825	0.2313	0.1877
r_{side}/a	0.3740	0.3129	0.2422	0.2195	0.1974	0.1598	0.1287
r_{pole}/a	0.3561	0.2998	0.2329	0.2112	0.1899	0.1536	0.1237
r_{back}/a	0.4050	0.3454	0.2746	0.2513	0.2283	0.1884	0.1547
r_{point}/r_{pole}	1.404	1.431	1.468	1.477	1.488	1.506	1.517

Table 7: Approximate values V_{rot} and q_{sph}, with Ca I λ6439 Å line for spherical star model ($P_{orb} = 2$ d).

i	K_v (km/s)	$\phi = 0.0$			$\phi = 0.25$			the phase-averaged values		
		FWHM,Å	V_{rot}	q_{sph}	FWHM,Å	V_{rot}	q_{sph}	FWHM,Å	V_{rot}	q_{sph}
q=2										
30^o	74.8	1.386	70.0	2.1	1.530	77.0	1.8	1.474	74.4	1.9
45^o	105.9	1.996	71.0	2.1	2.169	77.0	1.8	2.095	74.2	1.9
60^o	129.8	2.470	71.3	2.0	2.658	76.6	1.8	2.573	74.3	1.9
70^o	141.0	2.688	71.3	2.0	2.892	76.5	1.8	2.794	74.3	1.9
90^o	150.0	2.892	71.9	2.0	3.079	76.5	1.8	2.972	74.1	1.9
q=10										
30^o	158.1	1.360	68.6	11.4	1.531	77.0	8.5	1.459	73.7	9.5
45^o	223.8	1.949	69.2	11.2	2.168	76.9	8.6	2.072	73.5	9.6
60^o	274.1	2.413	69.8	11.0	2.656	76.6	8.6	2.543	73.3	9.7
70^o	141.0	2.688	71.3	10.9	2.892	76.5	8.7	2.794	74.3	9.7
90^o	316.6	2.817	70.3	10.8	3.072	76.4	8.7	2.937	73.1	9.8
q=20										
30^o	205.7	1.366	69.0	22.9	1.550	78.1	16.3	1.474	74.4	18.8
45^o	291.0	1.961	69.7	22.9	2.195	77.9	16.4	2.092	74.1	18.8
60^o	356.6	2.431	70.3	21.7	2.692	77.4	16.7	2.567	74.1	18.8
70^o	387.0	2.634	70.1	21.9	2.920	77.3	16.8	2.787	74.1	18.8
90^o	411.8	2.833	70.7	21.4	3.113	77.3	16.8	2.963	73.8	19.0
q=40										
30^o	263.6	1.378	69.6	44.9	1.571	79.2	31.0	1.490	75.1	36.1
45^o	372.9	1.977	70.3	43.6	2.226	79.0	31.3	2.115	74.9	36.4
60^o	456.9	2.451	70.8	42.7	2.726	78.4	32.0	2.817	74.9	36.4
70^o	495.8	2.676	71.0	42.4	2.958	78.4	32.0	2.817	74.9	36.4
90^o	527.6	2.857	71.2	42.1	3.154	78.5	31.8	2.926	74.7	36.7

Table 8: Approximate values V_{rot}^{disk} and q_{disk}, with Ca I λ6439 Å line for classical rotational broadening model ($P = 1$).

q	K_v (km/s)	V_{rot}^{Roche}	$\phi = 0.25$			the phase-averaged values		
			FWHM, Å	V_{rot}^{disk}	q_{disk}	FWHM, Å	V_{rot}^{disk}	q_{disk}
1	123.58	94.77	3.940	118.86	0.68	3.863	116.53	0.7
2	189.03	91.58	3.829	115.50	1.33	3.729	112.46	1.39
5	298.45	90.19	3.792	114.37	3.08	3.673	110.76	3.28
7	345.10	90.23	3.804	114.74	4.14	3.675	110.82	4.46
10	400.29	90.46	3.823	115.32	5.65	3.685	111.13	6.16
20	518.85	91.24	3.864	116.56	10.44	3.717	112.10	11.54
40	664.93	92.18	3.903	117.74	19.62	3.755	113.25	21.83